Withdrawal of a stratified fluid from a rotating channel

By N. ROBB McDONALD† AND JÖRG IMBERGER

Department of Civil and Environmental Engineering and Centre for Water Research,
University of Western Australia, Nedlands 6009, WA, Australia

The flow of a stratified fluid toward a line sink in a rotating channel of finite width and depth is studied. The withdrawal flow is shown to be established by a set of Kelvin shear waves trapped within a distance of Nh/fn from the right-hand side wall ($f > 0$) looking in the direction of propagation, where $n = 1, 2, \ldots$ is the vertical mode number. In addition there are a set of waves (Poincaré modes) which propagate away from the sink with a cross-channel modal structure. The withdrawal flow has a boundary-layer structure: far from the right-hand wall the flow resembles that of McDonald & Imberger (1991), whereas close to the right-hand wall the development of the vertical structure of the withdrawal flow resembles that of the non-rotating case due to the presence of Kelvin shear waves. In a narrow channel Kelvin shear waves dominate the establishment of the withdrawal flow. The withdrawal flow is investigated for large times compared to the inertial period, where it is shown that the width of the boundary layer is of the same order as the distance downstream from the sink. The flow within the boundary layer is unsteady as the withdrawal layer thickness δ continues to collapse indefinitely, while outside the boundary layer it is steady with $\delta \sim fL/N$, L being the horizontal lengthscale downstream from the sink. A scaling analysis is developed for the narrow channel case in which the cross-channel velocity can be ignored. The results are applied to actual field data, where it is shown that the effect of rotation may explain why previous non-rotating theories have been inaccurate in predicting withdrawal layer thickness.

1. Introduction

Owing to its importance to water quality engineering, the flow of a stratified fluid toward a sink has been extensively studied both theoretically and in the laboratory. In particular, engineers are interested in the vertical structure of the sink flow since this determines the water quality properties, such as the dissolved oxygen content, of the withdrawn fluid. (For a recent review of selective withdrawal, see Imberger & Patterson 1990). The studies have generally neglected the effect of rotation, on the grounds that the scale of most reservoirs is not sufficiently large for such effects to be important. However, as demonstrated in Ivey & Imberger (1978), when the results of these studies have been used to predict the withdrawal-layer thickness from given field data there has been disagreement between the predictions of the theory and observation. In particular Ivey & Imberger found that the two-dimensional theory of Imberger, Thompson & Fandry (1976) underpredicted the

† Present address: Robert Hooke Institute, The Observatory, Clarendon Laboratory, Parks Road, Oxford OX1 3PU, UK.

withdrawal-layer thickness. In an attempt to reconcile this discrepancy they proposed that instead of using laminar values for the transport coefficients, good agreement could be found by using values which were an order of magnitude higher than their laminar values, presuming that turbulent processes are important in the diffusion of momentum and stratifying species. In a later paper, Ivey & Blake (1985), suggested that the nature of the sink, a point sink rather than a line sink, may result in a larger withdrawal-layer thickness. However, an application of their results *overpredicts* the withdrawal-layer thickness (see §4). An alternative explanation, advanced by Imberger (1980), is that rotational effects may be responsible for the apparent thickening of the withdrawal layer.

The flow of a rotating stratified fluid toward a sink has received little attention in the literature despite its possible limnological and obvious oceanographical significance (see McDonald 1990 for an oceanographic example). Whitehead (1980) studied the flow of a rotating stratified fluid toward a point sink remote from any sidewalls and having axial symmetry. Using a hydraulic-type analysis he showed that rotation causes the withdrawal layer thickness to grow like $t^{\frac{1}{2}}$ where t is time. This prediction was confirmed with a series of laboratory experiments. Kranenburg (1980) also used axisymmetry to study the case where viscous diffusion of vorticity dominates and found that transport toward the sink was almost entirely in the bottom and interfacial Ekman layers.

Monismith & Maxworthy (1989) performed experiments on the withdrawal from a rotating stratified fluid in a rectangular container via a point sink located in one of the sidewalls. The sink flow was initiated from a quiescent state and they found that the flow was established by long-wavelength boundary-trapped Kelvin waves which they called Kelvin shear waves, a term also adopted in this paper. The Kelvin shear waves propagate cyclonically around the tank setting up an anticyclonic withdrawal layer in their wake. The flow eventually became unstable, owing to sidewall viscous boundary-layer separation, and broke down into a series of counter-rotating gyres. One main conclusion they reached was that there was no withdrawal layer thickening due to rotation within the parameter range of their experiments, i.e. the withdrawal-layer thickness is determined solely by non-rotating dynamics. They explained their results using scaling arguments based on point sink theory which showed that if $f < N$ then there will be no thickening of the withdrawal layer due to rotation.

Selective withdrawal theory may also be applied to outflows from straits such as the Strait of Gibraltar, where, owing to the large horizontal lengthscales involved, it is expected that rotational effects be important. Indeed, Hogg (1985) representing the Mediterranean outflow with a three-layer model for the stratification in a channel of slowly varying width and depth, showed that rotation produces anticyclonic circulation consistent with the observations of the Alboran Gyre. Whitehead (1985) constructed a laboratory model of the Mediterranean outflow using a two-layer fluid and incorporating realistic geometry. Selective withdrawal was observed in which rotational effects were clearly evident. In particular the uplift of the density surface exhibited lateral variation across the width of the straight and large gyres formed which were also consistent with observations.

The above examples show that rotation may, in some cases, have profound effects on the withdrawal flow but minimal effect in other cases. It is clear that the general withdrawal problem will depend on many factors such as the strength of the sink flow, the relative magnitude of stratification and rotation effects, the magnitude of the effective viscosity, etc. Even the assumed geometry and topography of the withdrawal domain will strongly influence the withdrawal flow.

In an attempt to address the general withdrawal problem which takes into account some of the above factors, McDonald & Imberger (1991) (hereafter referred to as MI) studied the flow of a rotating stratified fluid in an unbounded domain. Specifically, they looked at the initial-value problem of suddenly starting the sink flow and found that if $f < N$ the initial potential flow collapses to a horizontal withdrawal-layer structure. The collapse is eventually halted as baroclinic production of vorticity caused by bending of the isopycnals toward the sink is balanced by either advection of vorticity, viscous diffusion of vorticity or production of vorticity as vortex filaments are tilted by the sink flow. A classification scheme generalizing that of Imberger *et al.* (1976) for the non-rotating case based on two parameters was introduced to describe the possible steady states and the corresponding withdrawal-layer thicknesses. When Coriolis production of vorticity balances baroclinic production of vorticity (i.e. the thermal wind balance) it was shown that the withdrawal-layer thickness, δ, is given by $\delta \sim fL/N$, where L is the horizontal distance from the sink. This linear growth from the sink is faster than the $L^{\frac{1}{3}}$ growth for the viscous–buoyancy or the constant-thickness layer predicted by the buoyancy–inertial case. Hence, depending on the magnitude of f/N, which may be several orders of magnitude less than unity, and the distance from the sink, rotation has the potential to thicken the withdrawal layer. This is in contrast to the experimental findings of Monismith & Maxworthy (1989) for a point sink in a rectangular channel. When the theory of MI was used to predict the withdrawal-layer thickness of the Wellington Reservoir using the field data reported in Ivey & Imberger (1978), it was found that their theory predicted a withdrawal-layer thickness of an order magnitude greater than that observed.

A possible reason for the above discrepancies in the theory of MI when applied to field data is the neglect of side boundaries perpendicular to the axis of the sink. Such boundaries are present in any withdrawal problem involving reservoirs and also in outflows from straits and must, therefore, be incorporated in any realistic reservoir withdrawal study. Gill (1976) showed the dramatic effect that such sidewalls may have on the dynamics of a rotating fluid. In particular he studied the adjustment under gravity of an initial discontinuity in free-surface elevation in a rotating channel using the shallow-water equations for a single homogeneous layer, and showed that as the channel width went to zero rotational effects were suppressed. Further, he showed that the dynamics of fluid contained in a channel of finite width displayed characteristics common to the limiting cases of both infinite width (no sidewalls) and vanishing width. In the light of this, the failure of MI to predict the correct withdrawal-layer thickness may be due to the neglect of sidewalls.

Motivated by the above discussion, the withdrawal of a stratified fluid from a rotating semi-infinite channel is studied in this paper in order to determine the influence of sidewalls on the withdrawal problem. Throughout this study it is assumed that the channel is filled with a density-stratified fluid with constant buoyancy frequency N. Further, the channel rotates with uniform angular velocity $\frac{1}{2}f$ and it is assumed that $f \ll N$ as is the case in most naturally occurring situations. Before proceeding to an investigation of the influence of sidewalls, for the purposes of comparison, §2 examines the evolution of the withdrawal flow in a channel of finite height but of infinite width using an appropriate distribution of sinks of the type discussed in MI. Sidewalls are introduced in §3. The development of the withdrawal flow is examined and compared to the infinite-width case of §2. Section 4 examines the large-time behaviour of the withdrawal flow and the boundary-layer structure. On the basis of the results of the previous sections a scaling analysis for narrow

reservoirs is developed in §5. Conclusions are presented in §6 and are discussed in the context of the experimental results of Monismith & Maxworthy (1989).

2. Infinitely wide channel

To elucidate the role of internal wave radiation in establishing the withdrawal flow it is instructive to investigate the limiting case of a channel of infinite width (i.e. no sidewalls) but finite height $(-h \leqslant z \leqslant h)$ before proceeding to the case of finite width. In this case $-\infty < y < \infty$, a line sink of strength $q(t)$ extends across this distance, and the motion may thus be considered as two-dimensional as all flow variables become independent of the y-coordinate.

The analysis begins by looking at the time development of the sink flow. Initially the fluid is at rest in the channel and at time $t = 0$ the line sink is suddenly switched on. MI showed that nonlinear effects are initially confined to distance of $(q/N)^{\frac{1}{2}}$. Since this distance is typically less than the scale depth of the reservoir h, linear theory will, at least initially, be valid. The governing equations are then

$$u_x + w_z = 0, \tag{2.1}$$

$$\rho_0(u_t - fv) = -P_x, \tag{2.2}$$

$$v_t + fu = 0, \tag{2.3}$$

$$\rho_0 w_t = -P_z - g\rho, \tag{2.4}$$

$$\rho_t + w\rho_{0z} = 0. \tag{2.5}$$

Here u is the velocity component in the x-direction, w is the velocity component in the z-direction, v the azimuthal velocity along the axis of the sink, P is the pressure perturbation from hydrostatic pressure and $\rho(x, z, t)$ is the variation of the density from the undisturbed density $\rho_0(z)$. The density perturbation is assumed small relative to ρ_0. The buoyancy frequency N is defined by $N^2 = -(g/\rho_0)(d\rho_0/dz)$ and is assumed constant. The Boussinesq approximation is made, in which the density $\rho_0(z)$ in the above inertial terms is approximated by the density at the level of the sink, i.e. $\rho_0(z) \approx \rho_0(0)$. This is valid for $N^2h/g \ll 1$ where h is the vertical height of the channel. This is easily satisfied for a typical reservoir operation (Imberger 1972).

Rather than solving the above equations for the given channel domain, it proves easier to make use of the solution of MI for the unbounded case and use the method of images to construct the solution which satisfies the boundary conditions of no flow normal to the top and bottom of the channel. In particular, MI solved (2.1)–(2.5) in an unbounded domain with a sink at the origin using Laplace transforms in time, where the Laplace transform has the usual definition:

$$\bar{g}(s) = \int_0^\infty g(t)\,e^{-st}\,dt.$$

The velocity components (in Laplace space) are given by

$$\bar{u} = \frac{-1}{2\pi}\,\bar{q}(s)\left(\frac{s^2 + N^2}{s^2 + f^2}\right)^{\frac{1}{2}} \frac{x}{x^2 + \dfrac{s^2 + N^2}{s^2 + f^2}z^2}, \tag{2.6}$$

and

$$\bar{w} = \frac{-1}{2\pi}\,\bar{q}(s)\left(\frac{s^2 + N^2}{s^2 + f^2}\right)^{\frac{1}{2}} \frac{z}{x^2 + \dfrac{s^2 + N^2}{s^2 + f^2}z^2}. \tag{2.7}$$

Further, using (2.3) the transformed azimuthal velocity is determined:

$$\bar{v} = \frac{f}{2\pi s} \bar{q}(s) \left(\frac{s^2+N^2}{s^2+f^2}\right)^{\frac{1}{2}} \frac{x}{x^2 + \frac{s^2+N^2}{s^2+f^2} z^2}. \tag{2.8}$$

The azimuthal velocity is in a direction parallel to the axis of the sink and is a consequence of angular momentum conservation; fluid drawn toward the sink is required to increase its swirling velocity. The above solutions are discussed in detail in MI where it is shown that, for $f \ll N$, the flow collapses to a horizontal withdrawal layer where a steady state occurs in the (x, z)-plane when the Coriolis production of vorticity by vortex filament tilting balances baroclinic production of vorticity, i.e. the thermal wind balance. For such a balance it was shown that if L is the horizontal lengthscale the vertical scale or the withdrawal-layer scale is given by $\delta \sim fL/N$.

For horizontal planes located at $z = \pm h$, and with a sink at the origin, the method of images is used to satisfy the no-flow condition on each boundary. Thus, for every sink a distance ξ below a boundary there is a sink located at a distance ξ above the boundary. The volume flux needs to be adjusted since in the channel problem only positive values of x are considered here whereas the above expressions for the velocity components apply for positive and negative x. Effectively this means doubling the volume flux in (2.6)–(2.8), i.e. replacing q by $2q$. This leads to the following infinite series for the horizontal velocity:

$$\bar{u} = -\frac{\bar{q}(s)}{\pi} \sum_{k=-\infty}^{\infty} \frac{\left(\frac{s^2+f^2}{s^2+N^2}\right)^{\frac{1}{2}} x}{\frac{s^2+f^2}{s^2+N^2}x^2 + (z+2kh)^2} = -\frac{\bar{q}(s)}{\pi h} \sum_{k=-\infty}^{\infty} \frac{\left(\frac{s^2+f^2}{s^2+N^2}\right)^{\frac{1}{2}} \frac{x}{h}}{\frac{s^2+f^2}{s^2+N^2}\left(\frac{x}{h}\right)^2 + \left(\frac{z}{h}+2k\right)^2}. \tag{2.9}$$

Henceforth, it is assumed that a sink of constant strength q has been initiated from rest, so that $\bar{q}(s) = q/s$. Using the identity (which may be proved by showing that both the left-hand and right-hand sides have the same Fourier sine transform in x)

$$\frac{1}{\pi} \sum_{k=-\infty}^{\infty} \frac{x}{x^2 + (z+2k)^2} = \frac{1}{2} + \sum_{n=1}^{\infty} \cos(n\pi z) \exp(-n\pi x)$$

the expression for horizontal velocity is

$$\bar{u} = -\frac{q}{hs} \left\{ \frac{1}{4} + \frac{1}{2} \sum_{n=1}^{\infty} \exp\left[-n\pi \left(\frac{s^2+f^2}{s^2+N^2}\right)^{\frac{1}{2}} \frac{x}{h}\right] \cos\frac{n\pi z}{h} \right\}. \tag{2.10}$$

A similar expression may be obtained for the vertical velocity $\bar{w}$. Putting $f = 0$ in (2.10) (i.e. a stratified non-rotating fluid) the solution reduces to the horizontal velocity in Laplace space found by Pao & Kao (1974) for the withdrawal of a stratified fluid from a horizontal duct.

The horizontal velocity (2.10) is examined for times large compared to the buoyancy period, i.e. $t \gg N^{-1}$, which implies $s \ll N$. This is equivalent to saying that the withdrawal layer has collapsed to sufficient 'thinness' that the hydrostatic approximation may be employed. It is convenient to non-dimensionalize equation (2.10) using h as the vertical scale, Nh/f as the horizontal lengthscale, f^{-1} as the timescale, and q/h as the horizontal velocity scale. With this scaling, and the use of the hydrostatic approximation, the non-dimensional horizontal velocity is

$$\bar{u} = -\frac{1}{2s} - \sum_{n=1}^{\infty} \frac{1}{s} \exp[-n\pi x(s^2+1)^{\frac{1}{2}}] \cos(n\pi z). \tag{2.11}$$

The Laplace transform in the above expression is inverted in the Appendix. The result is

$$u(x, z, t) = -\frac{1}{2} - \sum_{n-1}^{\infty} \left[1 - n\pi x \int_0^{(t^2 - (n\pi x)^2)^{\frac{1}{2}}} \frac{J_1(\alpha)}{[\alpha^2 + (n\pi x)^2]^{\frac{1}{2}}} \, d\alpha \right] H(t - n\pi x) \cos(n\pi z),$$

$$(2.12)$$

where J_1 is the first-order Bessel function of the first kind. Thus for times large compared to the buoyancy period the velocity field evolves as a series of discrete fronts propagating with velocity $1/n\pi$ or in dimensional terms $Nh/n\pi$. This is analogous to the evolution of sink flow of a stratified non-rotating fluid in a horizontal duct discussed by Pao & Kao (1974). They described the flow in the linear hydrostatic limit by a series of long internal gravity waves (or shear waves as they are termed in the selective-withdrawal literature) propagating away from the sink with velocity $Nh/n\pi$, where the thickness of the withdrawal layer at any point is equal to the vertical wavelength of the most recent shear wave moving past that point. Equation (2.12) can be thought of as the shear waves of Pao & Kao modified by a Coriolis-induced factor in square brackets.

In the large-time limit the vertical scale changes from h to δ, the withdrawal-layer thickness, and the resulting flow is discussed in MI. Briefly, u and w reach steady state, v increases linearly with time and the withdrawal flow is governed by the thermal wind balance in the azimuthal vorticity equation, i.e. $f v_z \sim g \rho_x / \rho_0$.

3. Finite-width channel

Consider now a channel of finite width as shown in figure 1. The channel extends from $x = 0$ to ∞ and is bounded in the vertical by no-flow boundaries at $z = \pm h$. The sidewalls of the channel are located at $y = 0$ and W. A line sink at $x = z = 0$ stretches from $y = 0$ to W and has uniform strength per unit width of q m^2 s^{-1}. For the initial development of the flow from a state of rest the motion is governed by the linear equations of motion but now there is dependence of the flow variables on the transverse coordinate y. The equations of motion are then

$$u_x + v_y + w_z = 0, \tag{3.1}$$

$$\rho_0(u_t - fv) = -P_x, \tag{3.2}$$

$$\rho_0(v_t + fu) = -P_y, \tag{3.3}$$

$$\rho_0 w_t = -P_z - g\rho, \tag{3.4}$$

$$\rho_t + w\rho_{0z} = 0. \tag{3.5}$$

The symbols are defined in section 2 and the Boussinesq approximation has been made where the density ρ_0 is the density at the level of the sink $z = 0$. These equations are to be solved according to the boundary conditions

$$w = 0 \quad (z = \pm h); \qquad v = 0 \quad (y = 0, W);$$

$$u = -\frac{qH(t)}{h} \delta\left(\frac{z}{h}\right) \quad (x = 0); \qquad u \rightarrow -\frac{qH(t)}{2h} \quad \text{as} \quad x \rightarrow \infty;$$

where $H(t)$ is the Heaviside function. These boundary conditions correspond to no flow normal to the boundaries at the top and bottom of the channel and at the
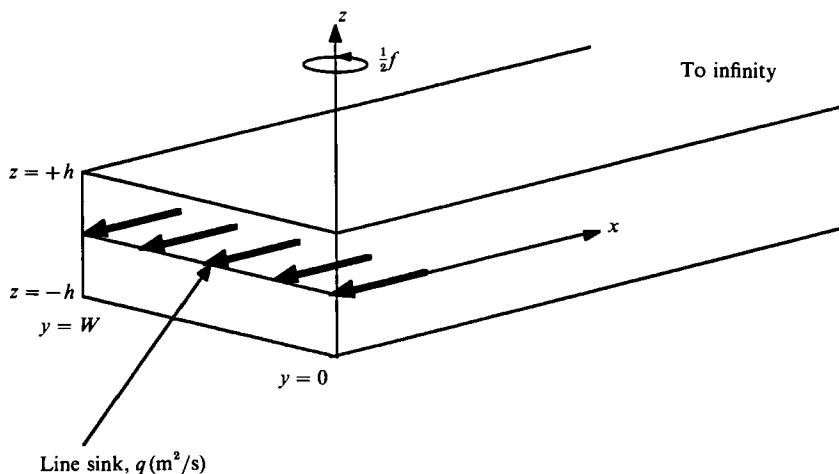
FIGURE 1. The channel geometry.

channel sidewalls. The condition at $x = 0$ represents a line sink across the channel at mid-height. Representation of the sink by a delta function is a mathematical convenience. A more realistic distributed sink would only affect the modal amplitudes of the shear waves (Monismith, Imberger & Billi 1988). The condition at large distances from the sink represents uniform flow toward the sink which is established instantaneously by the initial potential flow (see below).

Just after the sink flow has been turned on, rotation and stratification have no effect since their influence is manifested through forces proportional to the displacement of fluid particles which, initially, are zero. Hence, since the fluid is incompressible, the appropriate initial condition to use is that of potential flow and, in particular, the potential flow caused by a line sink in a horizontal duct (the sidewalls have no effect initially since $v = 0$). Denote this velocity potential by ϕ, so that at $t = 0$, $u = \phi_x$, $w = \phi_z$, $v = \rho = 0$, and define $P/\rho_0 = \phi + p$. The problem is now formulated in terms of p, the deviation of the pressure field divided by the mean density from the initial velocity potential. First, the Laplace transform of (3.1)–(3.5) is taken and the velocity components in Laplace space are found in terms of p. The results are

$$\bar{u} = \frac{-f\bar{p}_y - s\bar{p}_x}{s^2 + f^2}, \tag{3.6}$$

$$\bar{v} = \frac{f\bar{p}_x - s\bar{p}_y}{s^2 + f^2}, \tag{3.7}$$

$$\bar{w} = \frac{-s\bar{p}_z}{s^2 + N^2}. \tag{3.8}$$

The above velocity components are then substituted into the Laplace transformed version of the conservation of mass equation (3.1) to yield the following single equation for $\bar{p}$:

$$\bar{p}_{xx} + \bar{p}_{yy} + \frac{s^2 + f^2}{s^2 + N^2} \bar{p}_{zz} = 0. \tag{3.9}$$

The boundary conditions in terms of $\bar{p}$ are

$$\bar{p}_z = 0 \quad (z = \pm h), \tag{3.10}$$

$$f\bar{p}_x - s\bar{p}_y = 0 \quad (y = 0, W), \tag{3.11}$$

$$f\bar{p}_y + s\bar{p}_x \to (s^2 + f^2)\, q/2hs \quad (x \to \infty), \tag{3.12}$$

$$f\bar{p}_y + s\bar{p}_x = (s^2 + f^2)\, (q/hs)\, \delta(z/h) \quad (x = 0). \tag{3.13}$$

The task now reduces to solving (3.9) subject to boundary conditions (3.10)–(3.13). By virtue of the zero-gradient boundary condition (3.10) and (3.12), the following form of solution is tried for $\bar{p}$:

$$\bar{p} = \frac{q}{2hs}(sx + fy) + \sum_{n=1}^{\infty} \frac{q}{h} \phi_n(x, y) \cos \frac{n\pi z}{h}. \tag{3.14}$$

Here $\phi_n(x, y)$ (not to be confused with the velocity potential mentioned earlier) satisfies the Helmholtz equation

$$\phi_{nxx} + \phi_{nyy} - \gamma^2 \phi_n = 0, \quad \gamma^2 = \frac{n^2 \pi^2}{h^2} \frac{s^2 + f^2}{s^2 + N^2},$$

in the semi-infinite strip $0 \leqslant x < \infty$, $0 \leqslant y \leqslant W$, subject to

$$f\phi_{nx} - s\phi_{ny} = 0 \quad (y = 0, W), \tag{3.15}$$

$$\phi_n \to 0 \quad (x \to \infty), \tag{3.16}$$

$$f\phi_{ny} + s\phi_{nx} = (s^2 + f^2)/s \quad (x = 0). \tag{3.17}$$

In writing (3.17) the identity (Stakgold 1967, p. 51)

$$\delta(z/h) = \frac{1}{2} + \sum_{n=1}^{\infty} \cos \frac{n\pi z}{h}$$

has been used. A solution for ϕ_n satisfying (3.15) and (3.16) is

$$\phi_n = A_0 \exp\left[-\frac{n\pi}{h} \frac{sx + fy}{(s^2 + N^2)^{\frac{1}{2}}}\right] + \sum_{m=1}^{\infty} A_m \exp\left\{-\left(\frac{s^2 + f^2}{s^2 + N^2} \frac{n^2}{h^2} + \frac{m^2}{W^2}\right)^{\frac{1}{2}} \pi x\right\}$$

$$\times \left[\frac{-fW}{sm}\left(\frac{s^2 + f^2}{s^2 + N^2} \frac{n^2}{h^2} + \frac{m^2}{W^2}\right)^{\frac{1}{2}} \sin \frac{m\pi y}{W} + \cos \frac{m\pi y}{W}\right], \quad (3.18)$$

where the A_0 and A_m are to be determined from the boundary condition (3.17). Substitution of (3.18) into (3.17) yields the condition

$$1 = B_0 \exp\left[-\frac{n\pi}{h} \frac{fy}{(s^2 + N^2)^{\frac{1}{2}}}\right]$$

$$+ \sum_{m=1}^{\infty} B_m \left\{\cos \frac{m\pi y}{W} - \frac{fs}{s^2 + N^2} \frac{\sin(m\pi y/W)}{\left[\frac{s^2 + f^2}{s^2 + N^2} \frac{h^2 m^2}{n^2 W^2} + \frac{m^4 h^4}{n^4 W^4}\right]^{\frac{1}{2}}}\right\}, \quad (3.19)$$

where

$$B_0 = -\frac{sn\pi}{h(s^2 + N^2)^{\frac{1}{2}}} A_0 \tag{3.20a}$$

and

$$B_m = -\left[\frac{s^2 + f^2}{s^2 + N^2} \frac{n^2}{h^2} + \frac{m^2}{W^2}\right]^{\frac{1}{2}} \pi A_m. \tag{3.20b}$$

The task of finding the coefficients B_0 and B_m from (3.19) is difficult since the function involved in the curly brackets is not self-adjoint. This is a result of the 'oblique' derivative at the boundary condition specified by (3.11). However, for times large compared to the buoyancy period, i.e. $s \ll N$, it is clear the amplitude of the sine term in (3.19) is much less than the amplitude of the cosine term except, possibly, when $n/m \to \infty$. Fortunately, in this limit the terms in (3.18) involving A_m become exponentially small, for non-zero x, and are therefore unimportant. Thus the coefficients are evaluated with the understanding that $s \ll N$, or, equivalently, the hydrostatic limit, i.e. only the cosine expansion in (3.19), is found. Before the coefficients are evaluated, (3.18) and (3.19) are non-dimensionalized. Since large times only are being considered, as in §2, the Laplace transform variable is non-dimensionalized by f, the horizontal lengths x and y by Nh/f and the vertical lengthscale by h. Assuming then that $s \ll N$ this leaves one free parameter in the system $B = Wf/Nh$, i.e. the ratio of the width of the channel to the Rossby radius of deformation, Nh/f, of the primary ($n = 1$) mode. In terms of B, the coefficients are

$$B_0 = \frac{Bn\pi}{1 - \exp(-Bn\pi)} \tag{3.21a}$$

and

$$B_m = B_0 \frac{2Bn\pi}{B^2 n^2 \pi^2 + m^2 \pi^2} [\exp(-Bn\pi)(-1)^m - 1]. \tag{3.21b}$$

The transformed velocity in the x-direction, using (3.6) with $s \ll N$, is

$$\bar{u} = -\frac{1}{2s} - \sum_{n=1}^{\infty} \left[\frac{B_0}{s} \exp[-n\pi(sx+y)] \right.$$

$$\left. + \sum_{m=1}^{\infty} \frac{B_m}{s} \exp\left\{ -\left[s^2 + 1 + \frac{m^2}{n^2 B^2} \right]^{\frac{1}{2}} n\pi x \right\} \cos\frac{m\pi y}{B} \right] \cos(n\pi z). \tag{3.22}$$

The Laplace transform inversion of (3.22) can now be performed, using the Appendix, giving

$$u = -\frac{1}{2} - \sum_{n=1}^{\infty} \left[B_0 H(t-n\pi x) \exp[-n\pi y] + \sum_{m=1}^{\infty} B_m H(t-n\pi x) \right.$$

$$\left. \times \left\{ \left(1 - n\pi x \left(1 + \frac{m^2}{n^2 B^2} \right)^{\frac{1}{2}} \int_0^{(t^2-(n\pi x)^2)^{\frac{1}{2}}} \frac{J_1[(1+m^2/n^2 B^2)^{\frac{1}{2}} \alpha]}{[\alpha^2 + (n\pi x)^2]^{\frac{1}{2}}} d\alpha \right) \cos\frac{m\pi y}{B} \right\} \right] \cos(n\pi z). \tag{3.23}$$

The expression (3.23) for the horizontal sinkward velocity exhibits interesting behaviour. The first term represents the spectrum of shear waves of Pao & Kao (1974) modified by the factor $\exp(-n\pi y)$, i.e. an exponential cross-channel decay away from the wall at $y = 0$. These are in fact the Kelvin shear waves which were postulated to exist and observed experimentally by Monismith & Maxworthy (1989). Each mode propagates away from the sink at the appropriate long wave speed $1/n\pi$ (or, dimensionally, $Nh/n\pi$) with the wall ($y = 0$) on its right looking in the direction of propagation (for $f > 0$). For convenience, call this wall the right-hand wall and the wall at $y = W$ the left-hand wall. Each mode is trapped within a distance $1/n\pi$ (or, dimensionally, $Nh/fn\pi$), a distance of one Rossby radius of deformation, against the right-hand wall. In addition to the Kelvin shear waves there is a spectrum of waves represented by the second term in (3.23). These, as will be shown, are closely related

to the waves which establish the withdrawal flow in the infinite-width case, i.e. (2.12). They do not decay away from the wall but, rather, exhibit a cross-channel modal structure. Following Gill (1976) these are termed Poincaré waves.

Thus the picture obtained so far is that the withdrawal flow is initiated by a series of waves which propagate away from the sink with the appropriate long-wave speed. The presence of rotation causes a particular class of these waves to be trapped against the right-hand wall. The establishment of the withdrawal flow is similar to Gill (1976) who considered the adjustment under gravity in a rotating channel of an initial discontinuity in free-surface height. In fact the integral in (3.23) is, not surprisingly, similar to that in Gill's solution. Gill's analysis of the adjustment of an initial discontinuity in surface height uses the shallow-water equations (equivalent to the approximation $t \gg N^{-1}$ made here) and considers the propagation of the $n = 1$ mode only. The establishment of the withdrawal flow here proceeds similarly to Gill for the $n = 1$ mode: the combination of the Poincaré and Kelvin waves serves to shift the initially parallel and equidistant streamlines in the (x, z)-plane, to concentrate them against the right-hand wall. In this case, as each successive mode passes, the withdrawal current intensifies against the right-hand wall. The vertical lengthscale collapses from the channel height h to δ, the withdrawal-layer thickness, and thus (3.23), based on an infinite set of vertical modes with vertical scale h, is no longer a valid representation of the withdrawal flow. The very large-time $(t \gg f^{-1})$ behaviour is investigated in the next section.

Before looking at the large-time behaviour of the withdrawal flow it is instructive to investigate (3.23) in the limiting cases of very narrow and very wide channels. As the channel width B goes to zero it follows from (3.21 a, b) that, for a given mode n, $B_0 \to 1$ and $B_m \to 0$. Hence (3.23) reduces to

$$u(x, y, z, t) = -\frac{1}{2} - \sum_{n=1}^{\infty} H(t - n\pi x) \exp\left(-n\pi y/B\right) \cos\left(n\pi z\right). \qquad (3.24)$$

Except for the cross-channel decay factor $\exp\left(-n\pi y\right)$ this is precisely the solution found by Pao & Kao (1974) for the flow of a stratified non-rotating fluid toward a sink in a horizontal duct. Hence in the limit as the channel width goes to zero the transient flow is dominated by Kelvin shear waves and the cross-channel velocity is negligible.

For a given mode in the wide channel limit $B \to \infty$, (3.23) reduces to

$$u = -\frac{1}{2} - \sum_{n=1}^{\infty} H(t - n\pi x) \left\{ Bn\pi \exp\left[-n\pi y\right] \right.$$

$$\left. + \left[1 - n\pi x \int_0^{(t^2 - (n\pi x)^2)^{\frac{1}{2}}} \frac{J_1(\alpha)}{[\alpha^2 + (n\pi x)^2]^{\frac{1}{2}}} d\alpha\right] \cos\left(m\pi y\right) \right\} \cos\left(n\pi z\right). \qquad (3.25)$$

The solution obtained in the limit $B \to \infty$ is not the same as the solution for the infinitely wide case derived in §2. This is because even in the limit $B \to \infty$ there is still a wall at $y = 0$ on which the boundary condition $v = 0$ must be satisfied. However, in the wide channel limit, far enough from the sidewall boundary $y \gg 1$, the terms involving y in (3.25) become exponentially small and the solution for the horizontal velocity becomes identical to that derived in §2. Hence in the wide channel limit it is clear that a 'boundary layer' structure exists where, close to wall, Kelvin wave effects dominate and further from the right-hand wall the flow develops as in the infinitely wide case of §2.

Inspection of (3.23) shows that the sink flow never reaches steady state, since an infinite number of modes are generated. As $t \to \infty$ the solution presented in this section may be thought of as an outer solution since it is based on the large lengthscale h and ignores the small lengthscale δ, the withdrawal-layer thickness. Indeed, in the limit $t \to \infty$ it can be shown that the vertical velocity number vanishes and the horizontal flow is geostrophic, consistent with the outer view that fluid enters the sink from an infinitely thin layer at the level of the sink in a channel of depth h. Of interest here is the vertical structure of the withdrawal flow on a scale of the withdrawal-layer thickness. This is investigated in the next section.

4. Large-time behaviour

As the withdrawal flow collapses to a thin horizontal layer the vertical lengthscale changes from the channel height h to δ, the withdrawal-layer thickness. Hence at large times the behaviour of the withdrawal flow should be independent of the channel height. To model the large-time behaviour consider a channel of width W but now with no rigid lid or bottom. That is, the domain is unbounded in both the x- and z-directions, i.e. $-\infty < x < \infty$ and $-\infty < z < \infty$. Although the region $x < 0$ is not of interest, it is retained here to enable ease of solutions via Fourier transform. As will be seen, such a model will enable the boundary-layer nature of the withdrawal flow to be investigated. Rather than representing the sink in the boundary conditions as done previously, it proves to be convenient to represent the sink in the conservation of mass equation (3.1), viz.

$$u_x + v_y + w_z = -qH(t)\,\delta(x)\,\delta(z). \tag{4.1}$$

Proceeding as before, the Laplace transform in time is taken and the velocity components (3.6)–(3.80 are derived. Further it is assumed that $t \gg N^{-1}, f^{-1}$ or, equivalently, $s \ll N, f$. This has the effect of filtering out the fast-timescale inertio–gravity waves. Substitution of (3.6)–(3.8) into (4.1), yields an equation for $\bar{p}$:

$$\bar{p}_{xx} + \bar{p}_{yy} + \bar{p}_{z'z'} = \frac{qNf}{s^2}\delta(x)\,\delta(z'), \tag{4.2}$$

where $z' = Nz/f$. Equation (4.2) is to be solved subject to the condition that the velocity normal to the sidewalls at $y = 0$ and W vanish which, as before, in terms of p reads

$$f\bar{p}_x - s\bar{p}_y = 0 \quad (y = 0, W). \tag{4.3}$$

Since the domains is unbounded in the x- and z-directions and the forcing is contained in (4.1) then (3.12) and (3.13) are replaced by the condition that the velocity components vanish at large distances from the sink, i.e.

$$\bar{p}_x, \bar{p}_{z'} \to 0 \quad \text{as} \quad (x^2 + z'^2)^{\frac{1}{2}} \to \infty. \tag{4.4}$$

Solution of (4.2) proceeds by way of a double Fourier transform defined by

$$\bar{\bar{p}}(k, l) = \int_{-\infty}^{\infty} \int_{-\infty}^{\infty} \bar{p}(x, z')\,\mathrm{e}^{\mathrm{i}(kx + lz')}\,\mathrm{d}x\,\mathrm{d}z',$$

with the corresponding inverse

$$\bar{p}(k, l) = \frac{1}{4\pi^2} \int_{-\infty}^{\infty} \int_{-\infty}^{\infty} \bar{\bar{p}}(x, z')\,\mathrm{e}^{-\mathrm{i}(kx + lz')}\,\mathrm{d}k\,\mathrm{d}l.$$

Taking the Fourier transform of (4.2) and (4.3) gives the following equation set for $\bar{\bar{p}}$:

$$\left.\begin{array}{r}\bar{\bar{p}}_{yy} - (k^2 + l^2)\,\bar{\bar{p}} = qNf/s^2, \\ s\bar{\bar{p}}_y + fik\bar{\bar{p}} = 0 \quad (y = 0, W).\end{array}\right\} \tag{4.5}$$

Rather than solving (4.5) for $\bar{p}$ it proves simpler to first solve for $\bar{v}$ since the boundary conditions apply directly to v. The Fourier–Laplace transform of the cross-channel velocity obeys

$$\left.\begin{array}{r}\bar{\bar{v}}_{yy} - (k^2 + l^2)\,\bar{\bar{v}} = -qNik/s^2 \\ \bar{\bar{v}} = 0 \quad (y = 0, W).\end{array}\right\} \tag{4.6}$$

Equation (4.6) has solution

$$\bar{\bar{v}} = \frac{qN}{s^2}\frac{ik}{k^2+l^2}\left\{1 - \frac{\sinh\left[(k^2+l^2)^{\frac{1}{2}}y\right] + \sinh\left[(k^2+l^2)^{\frac{1}{2}}(W-y)\right]}{\sinh\left[(k^2+l^2)^{\frac{1}{2}}W\right]}\right\}. \tag{4.7}$$

Rather than inverting the Fourier transform in (4.6) for arbitrary W the main features of the withdrawal flow are evident in the wide channel limit, i.e. $W(k^2+l^2)^{\frac{1}{2}} \gg 1$ with $y/W \ll 1$. In this limit $\bar{\bar{v}}$ becomes

$$\bar{\bar{v}} = \frac{qN}{s^2}\frac{ik}{k^2+l^2}\{1 - \exp\left[-(k^2+l^2)^{\frac{1}{2}}y\right]\}. \tag{4.8}$$

The inverse Fourier transform can be calculated by substituting $k = r\cos\theta$, $l = r\sin\theta$ and integrating first with respect to r. Standard representations of Bessel functions (e.g. McLachlan 1955, p. 61) may then be used to perform the θ-integral. The inverse Laplace transform is straightforward and the final result for the cross-channel velocity is (in terms of the original variable z)

$$v = \frac{qNf^2t}{2\pi}\frac{x}{f^2x^2+N^2z^2}\frac{y}{(x^2+y^2+(N/f)^2z^2)^{\frac{1}{2}}}. \tag{4.9}$$

Several features are immediately obvious. The cross-channel velocity increases linearly with time as in MI. As $y \to 0$, i.e. close to the sidewall, v vanishes in accordance with the boundary condition. It is clear that v has a boundary-layer structure in the cross-channel direction in which the boundary-layer thickness scales as the downstream distance x. For distances $y \gg x$ the azimuthal velocity is independent of y and is identical to that described in MI. For $y \ll x$ the azimuthal velocity is small relative to that outside the boundary layer. The boundary-layer structure could be inferred directly from (4.8) where for $(k^2+l^2)^{\frac{1}{2}}y \gg 1$, implying $y \gg x$, the exponential part of (4.8) may be ignored and the resulting Fourier–Laplace inversion yields the azimuthal velocity of MI.

The factor $1/s^2$ in (4.7) indicates that the cross-channel velocity v increasing linearly with time is a general result and is independent of channel width. This result can be explained using the equation for the vertical component of the vorticity $\xi = v_x - v_y$ which, by eliminating P from the horizontal momentum equations (3.2) and (3.3) and using conservation of mass (3.1), satisfies $\xi_t = fw_z$, i.e. as vortex filaments in the withdrawal layer are drawn toward the sink they are compressed producing negative vorticity (Pedlosky 1979; Monismith & Maxworthy 1989). Vorticity production through this mechanism continues as vortex filaments drawn toward the sink are compressed in the withdrawal layer. In a real fluid the cross-channel velocity will eventually become steady through the action of viscous or nonlinear effects.

It is instructive to investigate the structure of the sinkward velocity u. To calculate u the cross-channel momentum equation is used, viz.

$$v_t + fu = -p_y.$$

Since v is already known for large times it remains to calculate p_y. From (4.5) and (4.7), in the wide channel limit, the Fourier–Laplace transform of p_y is given by

$$\bar{\bar{p}}_y = \frac{qN}{s^2} \frac{ikf}{(k^2+l^2)^{\frac{1}{2}}[s(k^2+l^2)^{\frac{1}{2}}-ikf]} \exp[-(k^2+l^2)^{\frac{1}{2}}y]. \qquad (4.10)$$

Instead of inverting this Fourier–Laplace transform in its present form, the task is simplified by making use of the boundary-layer nature of the withdrawal flow. At large distances from the wall $\bar{\bar{p}}_y$ is exponentially small and the primary balance in the cross-channel momentum equation is $v_t \sim fu$. In unsteady flow, close to the wall, by virtue of the no-flux boundary condition the azimuthal velocity is small and thus baroclinic vorticity production $g\rho_z$ cannot be balanced by the vortex tilting term fv_z, i.e. the thermal wind balance cannot be satisfied. This means that as vorticity continues to be produced by baroclinicity, inside the boundary layer the withdrawal layer continues to collapse beyond the steady-state thickness fx/N it attains outside the boundary layer. Thus, at large times it is expected that within the boundary layer the vertical scale is much smaller than the horizontal scale and therefore $k \ll l$ in the boundary layer. Such an assumption was also employed by Wong & Kao (1970) in determining the steady-state flow of a stratified fluid past an obstacle. Making the approximation $k \ll l$ in (4.10) and carrying out the Fourier inversion yields

$$\bar{p}_y = \frac{qN}{s\pi} \frac{y+sx/f}{(y+sx/f)^2+(N/f)^2 z^2} \quad (x > 0)$$

$$= 0 \quad (x < 0). \qquad (4.11)$$

The assumption that $s \ll f$ does not necessarily imply that p_y has become steady. From (4.11), for a given distance downstream x, the time taken for steady state to be reached depends on the distance y from the sidewall, i.e. steady state is reached when $t \gg x/(yf)$. Thus, for the times being considered here $(t \gg f^{-1})$ steady state is certainly reached outside the boundary layer but may still be unsteady within the boundary layer. The Laplace inversion of (4.11) yields for $x > 0$

$$p_y = \frac{qN}{\pi} \frac{y}{y^2+(N/f)^2 z^2} \left\{ 1 - \exp\left(-\frac{fty}{x}\right) \left[\cos\frac{Ntz}{x} - (z/y)\sin\frac{Ntz}{x} \right] \right\} \qquad (4.12)$$

and is zero for $x < 0$. Therefore at a given x the sinkward velocity is given by

$$u = -\frac{p_y}{f} - \frac{qN}{2\pi f} \frac{x}{x^2+(N/f)^2 z^2} \frac{y}{(x^2+y^2+(N/f)^2 z^2)^{\frac{1}{2}}} \quad (x > 0)$$

$$= -\frac{qN}{2\pi f} \frac{x}{x^2+(N/f)^2 z^2} \frac{y}{(x^2+y^2+(N/f)^2 z^2)^{\frac{1}{2}}} \quad (x < 0). \qquad (4.13)$$

The asymmetry in the sinkward velocity about $x = 0$ is because the Kelvin waves initiated by the sink propagate away from the sink with the wall on their right, i.e. Kelvin waves propagating toward a direction of decreasing x along $y = 0$ are not permissible (although, this direction is not of primary interest here). For $y \gg x$ the sinkward velocity u becomes that of MI. For $y \ll x$ the flow continues to collapse
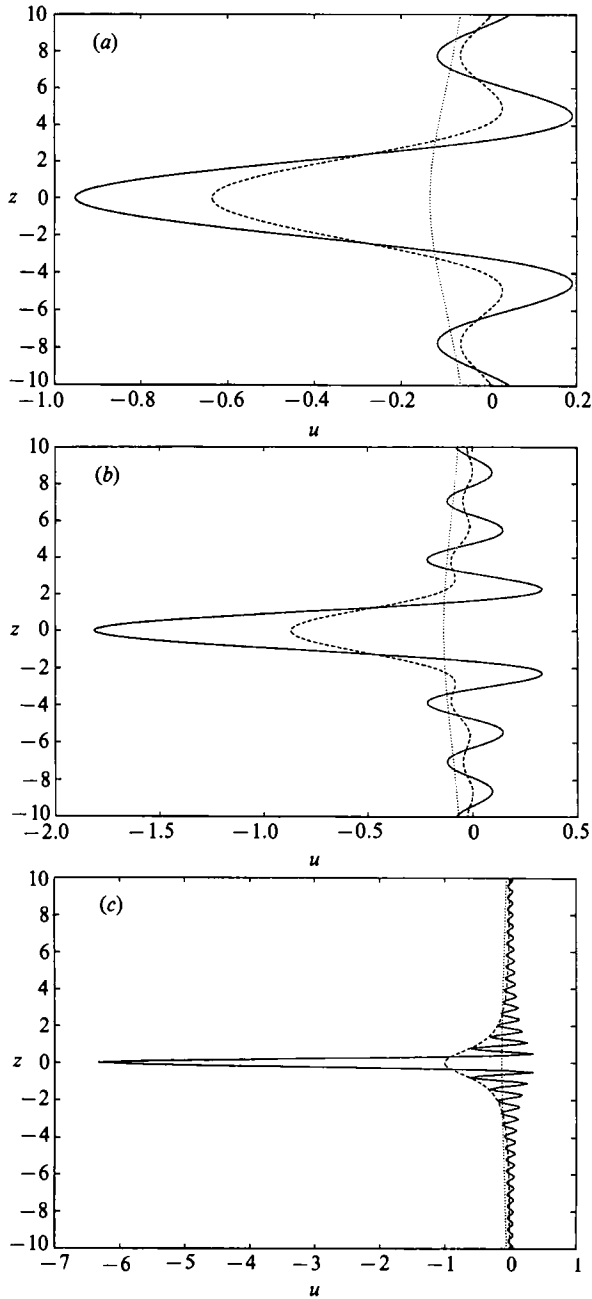
FIGURE 2. Sinkward velocity (non-dimensionalized by q/L) profiles at distance L from the sink for various cross-channel positions $y = 0.01L$ (——), (2) $y = 0.1L$ (---) and (3) $y = L$ (······). The graphs correspond to times (a) $ft = 10$, (b) $ft = 20$ and (c) $ft = 100$.

beyond a thickness of fx/N. This behaviour is illustrated in figure 2 which shows the velocity profile $u(z)$, non-dimensionalized by q/L, at $x = L$, where L is a lengthscale measuring the distance from the sink to the point of interest, for three different locations from the wall, namely, $y = 0.01L, 0.1L, L$. Each of the three plots, (a), (b) and (c), corresponds to a different time : $ft = 10, 20, 100$. At $ft = 10$ it is clear that the
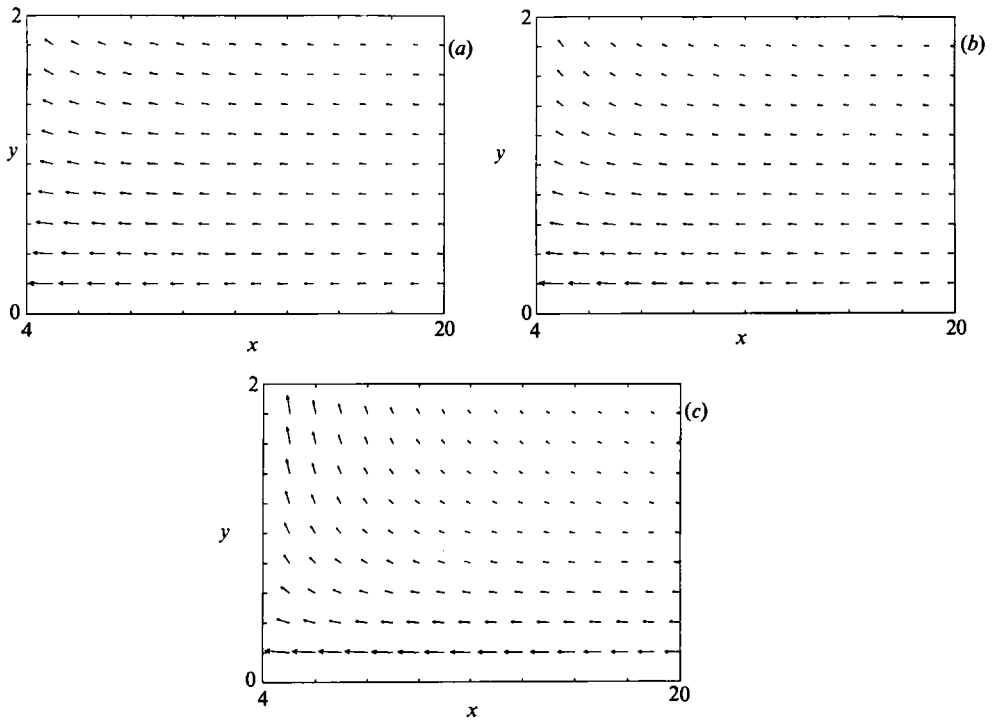
FIGURE 3. Horizontal velocity vectors (non-dimensionalized by q/L) at $z = 0$ in the domain $4L \leqslant x \leqslant 20L$ and $0 \leqslant y \leqslant 2L$. The graphs correspond to times $(a) ft = 10$, $(b) ft = 20$ and $(c) ft = 100$. The maximum arrow length in each figure gives the magnitude of the velocity field and corresponds to (a) 1.5, (b) 2.5, and (c) 4.0.

thickness of the withdrawal layer increases away from the right-hand wall. Also, the profile at $y = L$ shows no sign of transient behaviour since there are no regions of flow reversal, i.e. it has reached its steady state. This profile is the same as predicted by MI. At $ft = 20$, close to the wall at $y = 0.01L, 0.1L$ the withdrawal layer continues to collapse. The profile at $y = 0.1L$ is beginning to show signs of approaching a steady state as the magnitude of the oscillations decreases. At even larger times ($ft = 100$) the arrival of waves, given by (4.12), has produced a thin withdrawal layer at $y = 0.01L$ in which the fluid velocity toward the sink is large compared to its value outside the boundary layer. The situation is reminiscent of the non-rotating study of Pao & Kao (1974) who showed that the successive arrival of modes of smaller and smaller vertical wavelength produces a collapsing withdrawal layer of increasing velocity. At $y = 0.1L, L$ the withdrawal flow has reached a steady state.

The horizontal velocity field at $z = 0$ is illustrated in figure 3 in the domain $0 \leqslant y \leqslant 2L$, $4L \leqslant x \leqslant 20L$ for times $ft = 10, 20, 100$. At $ft = 10$ the sinkward velocity dominates everywhere. As time increases the cross-channel velocity increases linearly owing to comparison of vortex filaments as evident in figure 3(b) for $ft = 20$. The sinkward velocity also increases with time, but this increase is dependent on the (x, z) location (see (4.12)). At a given x the increase in the sinkward velocity is linear with time for $y \rightarrow 0$, but for large y the sinkward velocity is constant. The net effect is that the sinkward velocity continues to dominate the withdrawal flow in regions close to the right-hand wall but the cross-channel velocity becomes increasingly important further from the right-hand wall. This is made even more evident at much larger time $ft = 100$ in figure 3(c). At this time the cross-channel velocity has

increased sufficiently to be significant everywhere except in regions very close to the right-hand wall, i.e. $y \leqslant 0.2L$, and at distances further than $x = 20L$ from the sink. For example: if $y/x = 0.1$ then the cross-channel and sinkward velocities become comparable at time $ft = 200$, or about 20 days.

For very large times $ft \rightarrow \infty$ the sinkward velocity is steady everywhere and is given by

$$u = -\frac{qN}{f\pi} \frac{y}{y^2 + (N/f)^2 z^2} - \frac{qNf}{2\pi} \frac{x}{f^2 x^2 + N^2 z^2} \frac{y}{(x^2 + y^2 + (N/f)^2 z^2)^{\frac{1}{2}}} \quad (x > 0)$$

$$= -\frac{qNf}{2\pi} \frac{x}{f^2 x^2 + N^2 z^2} \frac{y}{(x^2 + y^2 + (N/f)^2 z^2)^{\frac{1}{2}}} \quad (x < 0). \tag{4.14}$$

From (4.14) in the limit $y \rightarrow 0$, $u \rightarrow -q\delta(z) H(x)$, i.e. for positive x, the withdrawal flow collapses to a line jet at the level of the sink as in the case of non-rotating stratified fluid.

To summarize, at a given location x at distances $y \gg x$ from the right-hand wall the dynamics resemble those described by MI. Close to the right-hand wall the withdrawal flow closely resembles that of Pao & Kao (1974), in that the withdrawal layer continues to collapse for times $t \geqslant f^{-1}$. This conclusion can be explained by appealing to Kelvin wave dynamics. Kelvin waves are trapped at the right-hand wall but may have frequencies much less than f. Specifically, the wave component of the solution (4.12) has frequency $\omega = fz/x$ and phase ωt. At the level of the sink $z = 0$ the Kelvin waves have the same phase and vanishing frequency and thus interfere constructively (see Bretherton 1967; MI) to produce large velocities at the level of the sink. Outside the boundary layer, and indeed on the left-hand wall, Kelvin waves have no influence and only inertio–gravity waves exist. Inertio–gravity waves have frequencies with a lower bound of f meaning a steady-state sinkward velocity is reached at times $t \sim f^{-1}$. For such times the thermal wind balance, $fv_z \sim g\rho_x/\rho_0$, still determines the withdrawal-layer thickness ($\delta \sim fL/N$) even though v vanishes on the left-hand wall since, from (3.2) and (3.4), ρ_x will also vanish in the same limit.

For a reservoir which can be modelled as a narrow channel of finite width W but extending infinitely far downstream from the sink, there will be some distance downstream x such that $x \gg W$ (i.e. the width of the boundary layer is greater than the width of the channel) and thus the ensuing dynamics will be governed predominantly by Kelvin wave dynamics. Thus for, say, the Wellington Reservoir, which has a mean width of 500 m (Ivey & Imberger 1978), at a distance of 5 km from the offtake the withdrawal dynamics are better described by Kelvin wave dynamics rather than the two-dimensional theory of MI. A scaling analysis incorporating these ideas is developed in the next section.

5. Scale analysis for a narrow channel

Consider a reservoir and let L be a measure of the distance from the sink to the point of observation and let W be the mean width of the reservoir. The previous sections showed that if $W \ll L$ then the withdrawal flow is established by Kelvin shear waves and, as a consequence, the cross-channel velocity is small and may be ignored. It is assumed the flow has become steady through the action of viscous or nonlinear effects. Moreover, steady state has been reached before the withdrawal flow has spun-up, via compression of vortex filaments, sufficiently for the cross-channel velocity to be important relative to the sinkward velocity. The transition between

the linear adjustment stage described in the previous sections to the steady-state investigated here is not studied. This transition has recently been investigated by Herman, Rhines & Johnson (1989) for the case of free-surface adjustment of a non-diffusive fluid where it was found that the nonlinear effect of vortex stretching favours anticyclonic circulation in the downstream half of the channel.

The various scales for the withdrawal-layer thickness at steady state under these conditions are now investigated. The vertical lengthscale is given by δ (i.e. the withdrawal-layer thickness), where $\delta \ll W, L$ the horizontal lengthscales in the y- and x-directions respectively. Under these conditions, together with the hydrostatic approximation, the governing equations are

$$u_x + w_z = 0, \tag{5.1}$$

$$uu_x + wu_z = -P_x/\rho_0 + \nu u_{zz}, \tag{5.2}$$

$$fu = -P_y/\rho_0, \tag{5.3}$$

$$0 = -P_z/\rho_0 - g\rho/\rho_0, \tag{5.4}$$

$$u\rho_x + w\rho_z = (N^2\rho_0/g)\,w + \kappa\rho_{zz}. \tag{5.5}$$

In the following scaling analysis the Prandtl number, $Pr = \nu/\kappa$, is assumed to be $O(1)$ as for temperature stratification.

The sink flow is driven by the along-channel pressure gradient and therefore (5.2) can always be assumed to be significant (see Condie & Ivey 1988, for a similar argument regarding an intrusion in a rotating stratified fluid).

First assume that convection of species dominates over diffusion of species in (5.5). This, in turn implies that convection of momentum also dominates over its diffusion by viscosity. This yields a scale for the perturbation density

$$\rho \sim \rho_0 N^2 \delta/g. \tag{5.6}$$

Eliminating P from (5.2) and (5.4) and using (5.6) and (5.1) gives

$$u \sim N\delta. \tag{5.7}$$

This is no more than the phase speed of an internal wave with vertical wavelength δ.

Now assume that the withdrawal flow is confined to a width b from the right-hand wall, where $b < W$. Further from the right-hand wall there is essentially no motion toward the sink. This situation is different to a very wide channel in which the cross-channel velocity is significant (zero by assumption) in which case the scaling of MI applies. Using b as the lateral (y) lengthscale, (5.3) and (5.4) combine to give

$$b \sim N\delta/f, \tag{5.8}$$

i.e. b is the Rossby radius of deformation of the Kelvin wave determining the withdrawal-layer thickness.

Conservation of mass requires $qW = b\delta u$ whence, using (5.7) and (5.8),

$$\delta \sim (qWf/N^2)^{\frac{1}{3}}. \tag{5.9}$$

The withdrawal layer is of constant thickness and, from (5.8), also of constant width.

If $b > W$, then W is the appropriate later scale and the withdrawal-layer thickness becomes

$$\delta \sim (q/N)^{\frac{1}{2}}. \tag{5.10}$$

This the thickness obtained by Imberger *et al.* (1976) for the non-rotating case. The withdrawal layer is uniform across the width of the channel. This result is expected

$\alpha > 1$	$R > 1$	$\delta \sim (q/N)^{\frac{1}{2}},$	$b \sim W$
	$R < 1$	$\delta \sim (\nu L/N)^{\frac{1}{3}},$	$b \sim W$
$\alpha < 1$	$R > \alpha$	$\delta \sim (fqW/N^2)^{\frac{1}{3}},$	$b \sim N\delta/f$
	$R < \alpha, \alpha < R^{\frac{1}{3}}$	$\delta \sim (\nu L/N)^{\frac{1}{3}},$	$b \sim N\delta/f$
	$R < \alpha, \alpha > R^{\frac{1}{3}}$	$\delta \sim (\nu L/N)^{\frac{1}{3}},$	$b \sim W$

TABLE 1. The various force balance regimes

since the Rossby radius of the Kelvin wave determining the withdrawal-layer thickness is greater than the channel width and hence rotation cannot be important.

Comparison of the withdrawal-layer thickness (5.9) and (5.10) yields the transition parameter

$$\alpha = (qN/W^2f^2)^{\frac{1}{3}}. \tag{5.11}$$

If, in (5.5), species dominates over species convection, then the following scale is obtained for the perturbation density:

$$\rho \sim \rho_0 N^2 \delta^2 w/g\kappa. \tag{5.12}$$

As before, elimination of P from (5.2) and (5.4) and substitution of (5.12) gives

$$\delta \sim (\nu L/N)^{\frac{1}{3}}. \tag{5.13}$$

Thus, unlike the inertially dominated case, the withdrawal-layer thickness is obtained immediately from the along-channel momentum equation (5.2) and is independent of rotational effects. Physically, this is because steady state is obtained through the action of viscosity dissipating the Kelvin waves. Thus only the vertical lengthscale over which viscosity acts is important in determining the steady-state withdrawal-layer thickness (Imberger 1980), not the horizontal velocity, and thus rotation does not influence the withdrawal-layer thickness. However, since δ increases like $L^{\frac{1}{3}}$ with distance from the sink then the sinkward velocity decreases within the withdrawal layer and thus it is expected that rotation influences the lateral scale of the withdrawal flow. In fact, using (5.3) the lateral lengthscale can be shown to again scale as the Rossby radius of deformation $b \sim N\delta/f$, where δ is given by (5.13). This gives a width which grows like $L^{\frac{1}{3}}$ downstream and eventually becomes uniform across the channel, when $b = W$ or $\alpha = R^{\frac{1}{3}}$. A Rossby radius which grows like $L^{\frac{1}{3}}$ is perhaps somewhat surprising but can be explained by realizing that the withdrawal layer in the buoyancy–diffusive balance consists of a continuous superposition of Kelvin waves of different vertical scales.

The scales for the withdrawal-layer thickness and length can be classified according to a two-parameter system R and α (see table 1), where $R = FGr^{\frac{1}{3}}$ is the parameter used by Imberger *et al.* (1976) and $\alpha = (qN/W^2f^2)^{\frac{1}{3}}$. The scaling scheme thus generalizes the scaling of Imberger *et al.* (1976) to include the effects of rotation in a narrow channel.

As an example illustrating the above scales consider the field data reported in Ivey & Imberger (1978). They measured the withdrawal layer at a distance of $L = 5$ km from the offtake and compared this with the theory of Imberger *et al.* (1976), with the appropriate values of the constants multiplying the scales determined numerically, or by experiment. They found the measured values of the withdrawal-layer thickness to be, on average, about a factor of two greater than that predicted by theory. They explained this discrepancy by postulating that the diffusion coefficients of momentum and temperature (the stratifying agent in this case) to be

a factor of 10 greater than that of their molecular values. Alternatively, the scaling arguments advanced in MI suggest the possibility of thickening of the withdrawal layer due to rotation without having to appeal to increased diffusion coefficients but their theory considerably overpredicted the withdrawal-layer thickness, owing to the neglect of sidewalls. Consider the value of δ calculated using the scaling scheme developed here. For the particular reservoir operation studied by Ivey & Imberger, the Wellington Reservoir has a mean width of $W = 500$ m, $q = 0.0134$ m s^{-1}, $N = 0.022$ s^{-1} and $f/N = 3.3 \times 10^{-3}$. At a distance of 5 km from the sink (so that $W \ll L$), using molecular values for the diffusivities, it is found that $R = 1.5$ and $\alpha = 0.6$ which implies from table 1 that

$$\delta \sim (fqW/N^2)^{\frac{1}{3}} = 1 \text{ m}, \quad b \sim 300 \text{ m}, \tag{5.14}$$

i.e. the withdrawal-layer thickness and width are influenced by rotation. Compare these values to the prototype values of $\delta = 2.5$–3.5 m and a mean width of 500 m (Ivey & Imberger 1978). Thus a dynamical balance in which rotation is important could explain the discrepancy between field data and non-rotating withdrawal theory. It should also be noted that the point sink theory of Ivey & Blake (1985) overpredicts the withdrawal-layer thickness in the case of the Wellington Reservoir data set (it gives $\delta = 4.7$ m). In the absence of a coefficient multiplying the scale estimate (5.8) and given the difficult nature of the field measurements, it is difficult to be more precise in stating whether rotation is important or not in determining the withdrawal-layer structure of the Wellington Reservoir. Indeed the values of R and α are very close to their critical values of unity. In a real reservoir situation other factors may also complicate the idealized model presented here. These include nonlinearity of the density profiles, topographic vortex stretching and vorticity sources other than planetary vorticity such as that introduced by wind stirring and river inflows.

6. Concluding remarks

The withdrawal of a stratified fluid from a rotating channel of finite width has been studied. Solution of a formal initial/boundary-value problem shows that the initial potential flow is modified by a series of waves with vertical wavelength h/n. One set of these waves (Kelvin shear waves) is trapped within a distance Nh/fn of the right-hand sidewall. In addition, there is another set of waves (Poincaré waves) which are analogous to waves which establish the withdrawal flow for the case where there are no sidewalls. As a consequence, the establishment of the withdrawal flow depends critically on its width. In a wide channel a boundary-layer structure exists where far from the right-hand wall, beyond the influence of Kelvin shear waves, the transient flow resembles that of MI. In a narrow channel Kelvin shear waves dominate the withdrawal flow establishment. The vertical structure of the withdrawal flow is investigated for large times compared to the inertial period and shows that the width of the boundary layer is of the same order as the distance downstream from the sink and the flow within the boundary layer is unsteady in that it continues to collapse while outside the boundary layer it is steady. The behaviour is explained in terms of Kelvin wave radiation, which may have frequencies less than f and, in particular, have vanishing frequency at the right-hand wall where a continuous superposition of Kelvin waves of the same phase leads to large velocities toward the sink.

The initial evolution of the flow examined using linear theory shows that the vertical lengthscale decreases with time, implying that both nonlinear and viscous

effects eventually become important. The ensuing steady flow is studied using scaling analysis incorporating both viscous and nonlinear effects. A classification scheme for withdrawal-layer thicknesses and widths is developed for narrow channels where the cross-channel velocity may be ignored relative to the sinkward velocity. This generalizes that of Imberger *et al.* (1976) in that it allows for the possibility of the sinkward velocity being in geostrophic balance with the cross-channel pressure gradient. It shows that if the parameter $\alpha = (qN/f^2 W^2)^{\frac{1}{3}}$ is less than unity then thickening of the withdrawal layer due to rotation is possible. The scaling scheme is applied to data obtained from the Wellington Reservoir (Ivey & Imberger 1978) and shows that rotation could be important in the withdrawal dynamics.

The above results can be related to the experiments performed by Monismith & Maxworthy (1989). There are some differences between the model used here and the experimental arrangement they used, namely the experimental tank they used was of finite length and a point sink is used rather than a line sink. As is shown here, they showed from their experimental results that Kelvin shear waves propagate away from the sink initiating the withdrawal flow. Owing to the finiteness of the tank, they propagate cyclonically around the perimeter of the tank, initiating an anticyclonic withdrawal flow. They observed that the flow field spins-up due to compression of vortex filaments by the falling free surface which produces negative vorticity. Negative vorticity is also produced in this model as vortex filaments are compressed in the withdrawal layer. It is this production of negative vorticity which is responsible for the breakup of the withdrawal flow into the series of counter-rotating gyres observed in the experiments of Monismith & Maxworthy. In any real fluid there will exist a viscous boundary layer on the sidewall in which the vorticity is positive, $\xi \sim -u_y$. When there is sufficient negative vorticity produced by vortex filament compression to match that in the viscous boundary layer, separation of sidewall viscous boundary layers into counter-rotating gyres will occur. Monismith & Maxworthy also attribute the observed instability in the withdrawal flow to positive vorticity in the viscous boundary layer.

Appendix. Laplace transform inversion of (2.11)

Consider the following Laplace transform:

$$\bar{g}(s) = \frac{1}{s} \exp\left[-a(s^2 + b^2)^{\frac{1}{2}}\right], \tag{A 1}$$

where $\bar{g}$ is the Laplace transform of $g(t)$. Rewrite (A 1) as

$$\bar{g}(s) = \frac{e^{-as}}{s} - \frac{1}{s}\left[e^{-as} - e^{-a(s^2 + b^2)^{\frac{1}{2}}}\right]. \tag{A 2}$$

In (A 2) denote the transform in the square brackets by $\bar{f}(s)$ and its inverse by $f(t)$. Inverting (A 2) yields, using elementary results of Laplace theory,

$$g(t) = H(t-a) - \int_0^t f(x)\,dx. \tag{A 3}$$

The inverse of $\bar{f}(s)$ can be found in Roberts & Kaufman (1966, p. 251) and is

$$f(t) = \frac{abJ_1[b(t^2-a^2)^{\frac{1}{2}}]}{(t^2-a^2)^{\frac{1}{2}}} H(t-a). \tag{A 4}$$

Substitution of (A 4) into (A 3) yields

$$g(t) = H(t-a)\left[1-ab\int_a^t \frac{J_1[b(x^2-a^2)^{\frac{1}{2}}]}{(x^2-a^2)^{\frac{1}{2}}}\mathrm{d}x\right]$$

$$= H(t-a)\left[1-ab\int_0^{(t^2-a^2)^{\frac{1}{2}}} \frac{J_1(b\alpha)}{(\alpha^2+a^2)^{\frac{1}{2}}}\mathrm{d}\alpha\right], \tag{A 5}$$

which is the result (2.12).

REFERENCES

BRETHERTON, F. P. 1967 The time dependent motion due to a cylinder moving in an unbounded rotating or stratified fluid *J. Fluid Mech.* **28**, 545–570.

CONDIE, S. A. & IVEY, G. N. 1988 Convectively driven coastal currents in a rotating basin. *J. Mar. Res.* **46**, 473–494.

GILL, A. E. 1976 Adjustment under gravity in rotating channel. *J. Fluid Mech.* **77**, 603–601.

HERMAN, A. J., RHINES, P. B. & JOHNSON, E. R. 1989 Nonlinear Rossby adjustment in a channel: beyond Kelvin waves. *J. Fluid Mech.* **205**, 469–502.

HOGG, N. G. 1985 Multilayer hydraulic control with application to the Alboran Sea circulation. *J. Phys. Oceanogr.* **15**, 454–466.

IMBERGER, J. 1972 Two-dimensional sink flow of a stratified fluid contained in duct. *J. Fluid Mech.* **53**, 329–349.

IMBERGER, J. 1980 Selective withdrawal: a review. In *2nd Intl Symp. on Stratified Flows, Trondheim*, p. 381.

IMBERGER, J. & PATTERSON, J. C. 1990 Physical limnology. *Adv. Appl. Mech.* **27**, 303–475.

IMBERGER, J., THOMPSON, R. & FANDRY, C. 1976 Selective withdrawal from a finite rectangular tank. *J. Fluid Mech.* **78**, 489–512.

IVEY, G. N. & BLAKE, S. 1985 Axisymmetric withdrawal and inflow in a density stratified container. *J. Fluid Mech.* **161**, 115–137.

IVEY, G. N. & IMBERGER, J. 1978 Field investigation of selective withdrawal. *J. Hydraul. Div. ASCE* **9**, 1225–1236.

KRANENBURG, C. 1980 Selective withdrawal from a rotating two layer fluid. In *IAHR Proc. Second Intl Symp. on Stratified Flows, Trondheim, Norway*, vol. 1, pp. 411–423.

McLACHLAN, N. W. 1955 *Bessel Functions for Engineers*. Oxford. 239 pp.

McDONALD, N. R. 1990 Far-field flow forced by the entrainment of a convective plane plume in a rotating stratified fluid. *J. Phys. Oceanogr.* **20**, 1791–1798.

McDONALD, N. R. & IMBERGER, J. 1991 A line sink in a rotating stratified fluid. *J. Fluid Mech.* **233**, 349–368 (referred to herein as MI).

MONISMITH, S. G., IMBERGER, J. & BILLI, G. 1988 Unsteady selective withdrawal from a line sink. *J. Hydraul. Div. ASCE* **114**, 1134–1152.

MONISMITH, S. G. & MAXWORTHY, T. 1989 Selective withdrawal and spin up of a rotating stratified fluid. *J. Fluid Mech.* **199**, 377–401.

PAO, H.-S. & KAO, T. W. 1974 Dynamics of establishment of selective withdrawal of a stratified fluid from a line sink. Part 1. Theory. *J. Fluid Mech.* **65**, 657.

PEDLOSKY, J. 1979 *Geophysical Fluid Dynamics*. Springer. 624 pp.

ROBERTS, G. E. & KAUFMAN, H. 1966 *Table of Laplace Transforms*. Saunders. 367 pp.

STAKGOLD, I. 1967 *Boundary Value Problems of Mathematical Physics*, Vol. 1. Macmillan. 340 pp.

WHITEHEAD, J. A. 1980 Selective withdrawal of a rotating stratified fluid. *Dyn. Atmos. Oceans* **5**, 123.

WHITEHEAD, J. A. 1985 A laboratory study of gyres and uplift near the Strait of Gibraltar. *J. Geophys. Res.* C**90**, 7045–7060.

WONG, K. K. & KAO, T. W. 1970 Stratified flow over extended obstacles and its application to topographical effect on vertical wind shear. *J. Atmos. Sci.* **27**, 884–889.